JME

Journal of Mining & Environment,
Vol.8, No.2, 2017, 237-253.
DOI: 10.22044/jme.2016.759

A boundary element/finite difference analysis of subsidence phenomenon due to underground structures

S.E. Mirsalari, M. Fatehi Marji*, J. Gholamnejad and M. Najafi

Department of Mining and Metallurgical Engineering, Yazd University, Yazd, Iran

Received 26 May 2016; received in revised form 24 October 2016; accepted 30 October 2016
Corresponding author: mohammad.fatehi@gmail.com (M. Fatehi Marji).

Abstract
Analysis of the stresses, displacements, and horizontal strains of the ground subsidence due to underground excavation in rocks can be accomplished by means of a hybridized higher order indirect boundary element/finite difference (BE/FD) formulation. A semi-infinite displacement discontinuity field is discretized (numerically) using the cubic displacement discontinuity elements (i.e. each higher order element is divided into four sub-elements bearing a cubic variation in the displacement discontinuities). Then the classical finite difference formulation (i.e. the backward, central, and forward finite difference formulations) is hybridized using the boundary element formulation, enabling us to obtain the nodal tangential stresses and horizontal strains along the elements. Several example problems are solved numerically, and the results obtained are then compared with their corresponding results available in the literature. These comparisons show the effectiveness and validness of the proposed method. A classical practical problem is also used to verify the applicability of the hybridized method.

Keywords: *Subsidence, Horizontal strain, Semi-infinite problems, Indirect boundary element method, Finite difference method, Higher order elements.*

1. Introduction

Theoretical and empirical modeling of the subsidence phenomenon on the surface of underground structures such as big coal mines have started since the late 1950's. The principal developments of these models are given by NCB (National Coal Board) [1]. Computer programs have been provided to perform multiple calculations of subsidence and its associated strains (for example, horizontal strains) [2, 3]. The reliability and accuracy of the prediction models can be judged based on the comparisons made with the field data gathered under different conditions by many investors from several countries [4]. Several numerical modelings such as the finite element method (FEM), finite difference method (FDM), and boundary element method (BEM) may be used to calculate the stress, displacement, and strain fields on the ground surfaces of a subsided area above underground excavations [5-10]. BEM has been widely used to solve many problems in various engineering fields such as the electrical, mechanical, civil, and mining ones [11-23].

Indirect BEM may be regarded as a kind of dual boundary element method [24] because the dual surfaces of a straight line cracking element are simultaneously considered in the elastic solution of solid substances, as explained by Crouch and Starfield (1983). The higher order displacement discontinuity method (which is a version of the indirect BEM) was originally developed for solving plane elasticity and fracture mechanics problems in finite, infinite, and semi-infinite domains [25-28]. In the present work, a hybridized form of the semi-infinite higher order displacement discontinuity and finite difference methods is proposed to calculate the stresses, displacements, and horizontal strains for a conventional subsided area due to underground excavations (e.g. a shallow circular excavation and a longwall coal mine).

The fundamental solution to the kernel of the displacement discontinuity method is the Kelvin solution. For the solution of a problem with finite dimensions (e.g. the semi-infinite shallow tunnel problem), the Kelvin solution cannot be used directly (because this solution is for a point source in an infinite domain). Therefore, some particular solutions can be added to it to model the stress free condition at the ground surface of a shallow tunnel (e.g. the image solution explained for the displacement discontinuity method by Crouch and Starfield (1983)). In this work, the higher order displacement discontinuity method is applied for semi-infinite problems using boundary elements with a cubic variation in the displacement discontinuities in order to solve the shallow tunnel problem. The tangential stresses along the boundary of the problem and also on its ground surface cannot be obtained as a direct solution to the displacement discontinuities by the Greens function theory. Thus the finite difference method was added to the solution to enable us to compute the tangential stresses on the boundary of the excavation and the horizontal stresses on the ground surface of the semi-infinite shallow tunnel problems. In order to get more accurate results for stresses and displacements, a cubic variation in displacement discontinuity was assumed along each boundary element.

In this work, the Mindlin solution was considered for a shallow circular cavity under the plane strain condition as an example problem of the shallow excavations [29]. Therefore, a 2D displacement discontinuity method was hybridized with the classical finite difference method using a cubic variation in the displacement discontinuity to estimate the tangential stresses along the boundary of the ground surface above an underground excavation.

To verify the applicability of the hybridized method for the subsidence analysis of underground coal mining (long-wall method), a classical practical problem was also solved numerically.

2. Hybridized higher order displacement discontinuity-finite difference formulation for semi-infinite plane elasticity problems

The constant displacement discontinuity D_i (D_x or D_y) is defined as the displacement between the two sides of a boundary element on the *x* axis, as [11]:

$$D_i = u_i(x,0^-) - u_i(x,0^+),\ i = x, y \tag{1}$$

In this research work, a cubic variation in displacement discontinuity along each boundary element (as shown in Figure 1) was used as what follows

$$\begin{aligned} &D_i(\varepsilon) = N_1(\varepsilon)D_i^1 + N_2(\varepsilon)D_i^2 + \\ &N_3(\varepsilon)D_i^3 + N_4(\varepsilon)D_i^4, \quad i = x, y \end{aligned} \tag{2}$$

where, D_i^1, D_i^2, D_i^3, and D_i^4 are the cubic nodal displacement discontinuities, and their four-related shape functions using equal sub-elements (i.e. $a_1 = a_2 = a_3 = a_4$) could be defined as what follow:

$$\begin{aligned} N_1(\varepsilon) &= -(3a_1^3 - a_1^2\varepsilon - 3a_1\varepsilon^2 + \varepsilon^3)/(48a_1^3),\\ N_2(\varepsilon) &= (9a_1^3 - 9a_1^2\varepsilon - a_1\varepsilon^2 + \varepsilon^3)/(16a_1^3),\\ N_3(\varepsilon) &= (9a_1^3 + 9a_1^2\varepsilon - a_1\varepsilon^2 - \varepsilon^3)/(16a_1^3),\\ N_4(\varepsilon) &= -(3a_1^3 + a_1^2\varepsilon - 3a_1\varepsilon^2 - \varepsilon^3)/(48a_1^3) \end{aligned} \tag{3}$$

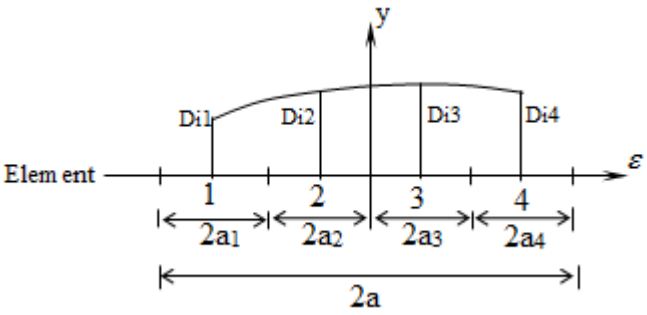

Figure 1. Cubic displacement discontinuity variation along a boundary element of length 2a.

The displacements and stresses for a line crack in an infinite body along the x-axis in terms of the single harmonic functions *g(x,y)* and *f(x,y)* are [11]:

$$\begin{aligned} u_x &= \left[2(1-\nu)f_{,y} - yf_{,xx}\right] + \left[-(1-2\nu)g_{,x} - yg_{,xy}\right]\\ u_y &= \left[(1-2\nu)f_{,x} - yf_{,xy}\right] + \left[2(1-\nu)g_{,y} - yg_{,yy}\right] \end{aligned} \tag{4}$$

and the stresses are:

$$\begin{aligned} \sigma_{xx} &= 2\mu\left[2f_{,xy} + yf_{,xyy}\right] + 2\mu\left[g_{,yy} + yg_{,yyy}\right]\\ \sigma_{yy} &= 2\mu\left[-yf_{,xyy}\right] + 2\mu\left[g_{,yy} - yg_{,yyy}\right]\\ \sigma_{xy} &= 2\mu\left[2f_{,yy} + yf_{,yyy}\right] + 2\mu\left[-yg_{,xyy}\right] \end{aligned} \tag{5}$$

where μ is the shear modulus, and $f_{,x}, g_{,x}, f_{,y}, g_{,y}$, etc. are the partial derivatives of the single harmonic functions *f(x,y)* and *g(x,y)* with respect to x and y, in which these potential functions for the cubic element case can be found from:

$$\begin{aligned} f(x,y) &= \frac{-1}{4\pi(1-\nu)}\sum_{j=1}^{4} D_x^j F_j(I_i),\ i = 1 \text{ to } 4\\ g(x,y) &= \frac{-1}{4\pi(1-\nu)}\sum_{j=1}^{4} D_y^j F_j(I_i),\ i = 1 \text{ to } 4 \end{aligned} \tag{6}$$

in which, the common function, $F_j(I_i)$, can be defined as:

$$F_j(I_i) = \int N_j(\varepsilon)\ln\left[(x-\varepsilon)+y^2\right]^{\frac{1}{2}}d\varepsilon, \quad j=1 \text{ to } 4,\ i=1 \text{ to } 4 \tag{7}$$

where the integrals I_1, I_2, I_3, and I_4 can be expressed as:

$$I_1(x,y) = \int_{-a}^{a} \ln\left[(x-\varepsilon)^2+y^2\right]^{\frac{1}{2}}d\varepsilon = y(\theta_1-\theta_2) - (x-a)\ln(r_1) + (x+a)\ln(r_2) - 2a \tag{8-a}$$

$$I_2(x,y) = \int_{-a}^{a} \varepsilon\ln\left[(x-\varepsilon)^2+y^2\right]^{\frac{1}{2}}d\varepsilon = xy(\theta_1-\theta_2) + 0.5\left(y^2-x^2+a^2\right)\ln\frac{r_1}{r_2} - ax \tag{8-b}$$

$$I_3(x,y) = \int_{-a}^{a} \varepsilon^2\ln\left[(x-\varepsilon)^2+y^2\right]^{\frac{1}{2}}d\varepsilon = \frac{y}{3}(3x^2-y^2)(\theta_1-\theta_2) + \frac{1}{3}(3xy^2-x^3+a^3)\ln(r_1) - \frac{1}{3}(3xy^2-x^3-a^3)\ln(r_2) - \frac{2a}{3}(x^2-y^2+\frac{a^2}{3}) \tag{8-c}$$

$$I_4(x,y) = \int_{-a}^{a} \varepsilon^3\ln\left[(x-\varepsilon)^2+y^2\right]^{\frac{1}{2}}d\varepsilon = -xy(x^2-y^2)(\theta_1-\theta_2) + 0.25(3x^4-6x^2y^2 + 8a^2x^2+a^4-y^4)\left[\ln(r_1)-\ln(r_2)\right] - 2ax(x^2+a^2)\left[\ln(r_1)+\ln(r_2)\right] + 1.5ax^3 - 3axy^2 + 7a^3x/6 \tag{8-d}$$

The terms θ_1, θ_2, r_1, and r_2 in this equation are defined as follow:

$$\theta_1 = \arctan(\frac{y}{x-a}),\quad \theta_2 = \arctan(\frac{y}{x+a}),\quad r_1 = \left[(x-a)^2+y^2\right]^{\frac{1}{2}}, and\ r_2 = \left[(x+a)^2+y^2\right]^{\frac{1}{2}} \tag{9}$$

The partial derivatives of the constant, linear, and quadratic integrals I_1, I_2, I_3 are given in the literature [18], and the partial derivatives of the cubic integral I_4 are given in appendix A for completeness.

Considering the typical elements i and j along the boundary of the problem and the elemental shear and normal boundary conditions b_s^i and b_n^i corresponding to the influence coefficients $C_{ss}(i,j)$, $C_{sn}(i,j)$, $C_{ns}(i,j)$, $C_{ns}(i,j)$, the general solution to the problem can be given as [11]:

$$b_s^i = \sum_{j=1}^{N} C_{ss}(i,j)D_s^i + \sum_{j=1}^{N} C_{sn}(i,j)D_n^j,\ i=1 \text{ to } N$$
$$b_n^i = \sum_{j=1}^{N} C_{ns}(i,j)D_s^i + \sum_{j=1}^{N} C_{nn}(i,j)D_n^j,\ i=1 \text{ to } N \tag{10}$$

The vertical displacement (surface subsidence) can be obtained as a solution to this equation for the surface elements. The horizontal strains on the surface can be obtained by applying the finite difference formulae to the following elastic formula for the horizontal and vertical stress components, as:

$$\sigma_{xx} = \frac{2G}{1-2\nu}[(1-\nu)e_{xx} + \nu e_{yy}]$$
$$\sigma_{yy} = \frac{2G}{1-2\nu}[\nu e_{xx} + (1-\nu)e_{yy}] \tag{11}$$

where G is the shear modulus, and e_{xx} and e_{yy} are the horizontal and vertical strain components, respectively. Considering a positive and negative side for the line crack elements, the following relations can be readily deduced:

$$\sigma_{xx}^{+} = \frac{2G}{1-\nu}e_{xx}^{+} + \frac{\nu}{1-\nu}\sigma_{yy}^{+}$$
$$\sigma_{xx}^{-} = \frac{2G}{1-\nu}e_{xx}^{-} + \frac{\nu}{1-\nu}\sigma_{yy}^{-} \tag{12}$$

The horizontal strain components are the derivatives of the displacements, as:

$$e_{xx}^{+} = \frac{\partial u_x^{+}}{\partial x},\quad e_{xx}^{-} = \frac{\partial u_x^{-}}{\partial x} \tag{13}$$

Combining Equations (12) and (13), the horizontal strain components may be obtained through the following formula:

$$\sigma_{xx}^{-} - \sigma_{xx}^{+} = \frac{2G}{1-\nu}\frac{\partial}{\partial x}(u_x^{-} - u_x^{+}) = \frac{2G}{1-\nu}\frac{\partial}{\partial x}(D_x) \tag{14}$$

where D_x is the horizontal displacement discontinuity component, and this differential form of D_x can be solved numerically using the finite difference formulae considering the first, central, and last elements along the boundary where the horizontal strain is to be calculated.

To solve the shallow tunnel problem, the boundary of the problem can be divided into a limited number of equal-sized displacement discontinuity elements, numbered from left to right. In order to find the tangential stresses $\overset{i}{\sigma}_{xx}^{+}$ and $\overset{i}{\sigma}_{xx}^{-}$ at the i^{th} element of the boundary, the derivatives (or the horizontal strains) $e_{xx}^{+} = \frac{\partial u_x^{+}}{\partial x}$ and $e_{xx}^{-} = \frac{\partial u_x^{-}}{\partial x}$ at this element must be calculated. This is

accomplished using the standard finite difference method. If function $f(x)$ stands for either u_x^+ or u_x^-, the three separate finite difference formulae for $\frac{\partial}{\partial x} f(x)$ at the point $x = \overset{i}{x}$ can be written as what follow.

The forward difference formula is:

$$(\frac{\partial f}{\partial x})_{x=x^i} = \frac{f(x^{i+1}) - f(x^i)}{x^{i+1} - x^i} \quad (15)$$

the central difference formula is:

$$(\frac{\partial f}{\partial x})_{x=x^i} = \frac{f(x^i) - f(x^{i-1})}{x^i - x^{i-1}} \quad (16)$$

and the backward difference formula is:

$$(\frac{\partial f}{\partial x})_{x=x^i} = \frac{f(x^{i+1}) - f(x^{i-1})}{x^{i+1} - x^{i-1}} \quad (17)$$

The numerical analysis of the plane elasticity problems in finite, infinite, and semi-infinite bodies can be accomplished by programming the above formulation based on the general structure given in Equation (10). The solution to the subject problem in a semi-infinite region $y \le 0$ can be obtained using Figure 2. The origin of the local $\bar{x}$ and $\bar{y}$ coordinate system is at the point $x = c_x, y = -c_y$. The analytical solution to this problem is obtained using the procedure known as the method of images [11]. Omitting the details of the solution, the complete solution for the half-plane $y \le 0$ can be summarized as:

$$u_i = u_i^{\mathrm{A}} + u_i^{\mathrm{I}} + u_i^{\mathrm{S}}$$
$$\sigma_{ij} = \sigma_{ij}^{\mathrm{A}} + \sigma_{ij}^{\mathrm{I}} + \sigma_{ij}^{\mathrm{S}} \quad (18)$$

in which u_i^{A}, σ_{ij}^{A} are the displacements and stresses due to the actual displacement discontinuity, u_i^{I}, σ_{ij}^{I} are those due to the images, and u_i^{S}, σ_{ij}^{S} are those resulting from the supplementary solutions, respectively.

The numerical analysis of plane elasticity problems in finite, infinite and, semi-infinite bodies can be accomplished by programming the above formulation based on the general structure of the boundary element method [11, 25]. The general solution and complete formulation for the higher order (cubic elements) displacement discontinuity method for half-plane problems is given in the following section.

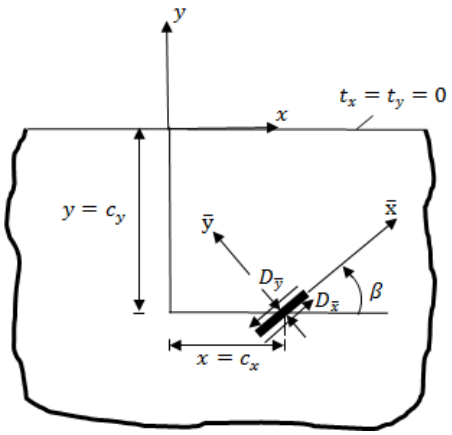

Figure 2. Displacement discontinuity in a half-plane $y \le 0$ [11].

2.1. Actual solutions to displacements and stresses

The analytical solution to a constant element displacement discontinuity over the line segment $|x| \le a$, $y = 0$ in the semi-infinite region $y \le 0$ (Figure 3) has already been introduced by Crouch and Starfield (1983).

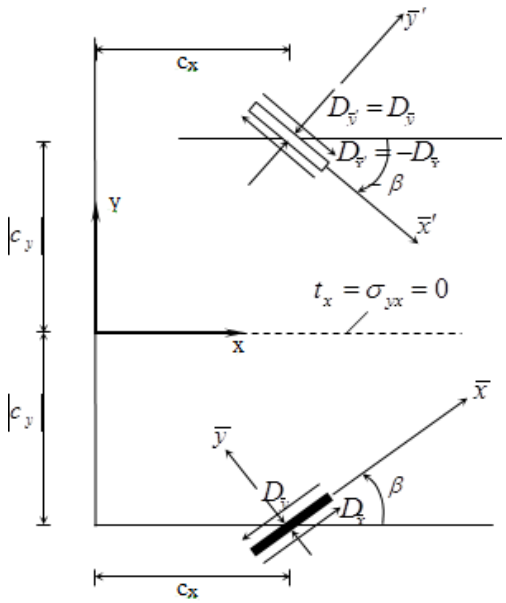

Figure 3. Actual and image displacement discontinuities in half-plane $y \le 0$ [11].

The displacements and stresses due to the actual displacement discontinuity are denoted by u_i^A and σ_{ij}^A; those due to its image, by u_i^I and σ_{ij}^I; and those resulting from the supplementary solution, by u_i^S and σ_{ij}^S. The complete solutions to the semi-infinite plane $y \le 0$ can be written as:

$$\begin{aligned} u_i &= u_i^A + u_i^I + u_i^S \\ \sigma_{ij} &= \sigma_{ij}^A + \sigma_{ij}^I + \sigma_{ij}^S \end{aligned} \tag{19}$$

Considering the geometry shown in Figure 3, the displacements and stresses due to the actual displacement discontinuities may be written using the results explained for the finite and infinite planes case. The local $\bar{x}, \bar{y}$ coordinates are related to the global *x*, *y* coordinates by the following two transformation formulae:

$$\begin{aligned} \bar{x} &= (x - c_x)\cos\beta + (y - c_y)\sin\beta \\ \bar{y} &= -(x - c_x)\sin\beta + (y - c_y)\cos\beta \end{aligned} \tag{20}$$

Denoting the common potential function $F_j(x, y)$ by $\overset{A}{F}_j(\bar{x}, \bar{y}) = \overset{A}{F}_{j1}$ and its derivatives by $\overset{A}{F}_{j,\bar{x}} = \overset{A}{F}_{j2}$, $\overset{A}{F}_{j,\bar{y}} = \overset{A}{F}_{j3}$, $\overset{A}{F}_{j,\bar{x}\bar{y}} = \overset{A}{F}_{j4}$, $\overset{A}{F}_{j,\bar{x}\bar{x}} = -\overset{A}{F}_{j,\bar{y}\bar{y}} = \overset{A}{F}_{j5}$, $\overset{A}{F}_{j,\bar{x}\bar{y}\bar{y}} = \overset{A}{F}_{j6}$, $\overset{A}{F}_{j,\bar{y}\bar{y}\bar{y}} = \overset{A}{F}_{j7}$, etc. for the actual displacement discontinuities, their cubic element formulations in terms of the global *x*, *y* coordinates are:

$$\begin{aligned} \overset{A}{u}_x = \frac{-1}{4\pi(1-\nu)} \sum_{J=1}^{4} \{ & [-(1-2\nu)\sin\beta \overset{A}{F}_{j2} + 2(1-\nu)\cos\beta \overset{A}{F}_{j3} + \bar{y}(\sin\beta \overset{A}{F}_{j4} - \cos\beta \overset{A}{F}_{j5})] D_{\bar{x}}^{j} + [-(1-2\nu)\cos\beta \overset{A}{F}_{j2} - \\ & 2(1-\nu)\sin\beta \overset{A}{F}_{j3} - \bar{y}(\cos\beta \overset{A}{F}_{j4} + \sin\beta \overset{A}{F}_{j5})] D_{\bar{y}}^{j} \} \end{aligned} \tag{21-a}$$

$$\begin{aligned} \overset{A}{u}_y = \frac{-1}{4\pi(1-\nu)} \sum_{J=1}^{4} \{ & [(1-2\nu)\cos\beta \overset{A}{F}_{j2} + 2(1-\nu)\sin\beta \overset{A}{F}_{j3} - \bar{y}(\cos\beta \overset{A}{F}_{j4} + \sin\beta \overset{A}{F}_{j5})] D_{\bar{x}}^{j} + [-(1-2\nu)\sin\beta \overset{A}{F}_{j2} + 2(1-\nu)\cos\beta \overset{A}{F}_{j3} - \\ & \bar{y}(\sin\beta \overset{A}{F}_{j4} - \cos\beta \overset{A}{F}_{j5})] D_{\bar{y}}^{j} \} \end{aligned} \tag{21-b}$$

The actual stresses are:

$$\overset{A}{\sigma}_{xx} = \frac{-2G}{4\pi(1-\nu)} \sum_{j=1}^{4} \{ [2\cos^2\beta \overset{A}{F}_{j4} + \sin 2\beta \overset{A}{F}_{j5} + \bar{y}(\cos 2\beta \overset{A}{F}_{j6} - \sin 2\beta \overset{A}{F}_{j7})] D_{\bar{x}}^{j} + [-\overset{A}{F}_{j5} + \bar{y}(\sin 2\beta \overset{A}{F}_{j6} + \cos 2\beta \overset{A}{F}_{j7})] D_{\bar{y}}^{j} \} \tag{22-a}$$

$$\overset{A}{\sigma}_{yy} = \frac{-2G}{4\pi(1-\nu)} \sum_{j=1}^{4} \{ [2\sin^2\beta \overset{A}{F}_{j4} - \sin 2\beta \overset{A}{F}_{j5} - \bar{y}(\cos 2\beta \overset{A}{F}_{j6} + \sin 2\beta \overset{A}{F}_{j7})] D_{\bar{x}}^{j} + [-\overset{A}{F}_{j5} - \bar{y}(\sin 2\beta \overset{A}{F}_{j6} + \cos 2\beta \overset{A}{F}_{j7})] D_{\bar{y}}^{j} \} \tag{22-b}$$

$$\overset{A}{\sigma}_{xy} = \frac{-2G}{4\pi(1-\nu)} \sum_{j=1}^{4} \{ [\sin 2\beta \overset{A}{F}_{j4} - \cos 2\beta \overset{A}{F}_{j5} + \bar{y}(\sin 2\beta \overset{A}{F}_{j6} + \cos 2\beta \overset{A}{F}_{j7})] D_{\bar{x}}^{j} + [-\bar{y}(\cos 2\beta \overset{A}{F}_{j6} - \sin 2\beta \overset{A}{F}_{j7})] D_{\bar{y}}^{j} \tag{22-c}$$

Displacements and stresses due to image and supplementary displacement discontinuity can be expressed in terms of the single function $\overset{I}{F}_j(\bar{x}', \bar{y}')$ and its derivatives, in which the image local $\bar{x}', \bar{y}'$ coordinates (as shown in Figure 3) are related to the *x*, *y* coordinates by the following transformation formulae:

$$\begin{aligned} \bar{x}' &= (x - c_x)\cos\beta - (y + c_y)\sin\beta \\ \bar{y}' &= (x - c_x)\sin\beta + (y + c_y)\cos\beta \end{aligned} \tag{23}$$

The two types of boundary conditions usually considered in plane elasticity problems, i.e. the shear and normal stresses boundary conditions $\sigma_s^i = (\sigma_s^i)_0$, $\sigma_n^i = (\sigma_n^i)_0$ and the shear and normal displacements boundary conditions $u_s^i = (u_s^i)_0$, $u_n^i = (u_n^i)_0$, in which $(\sigma_s^i)_0$, $(u_s^i)_0$, etc., are the given boundary values for the stresses and displacements corresponding to the local $\bar{x}, \bar{y}$ coordinates shown in Figure 3, respectively [12, 14]. These boundary conditions are defined at the center of each four-element patch so that finally, a system of 2(N = 4N) algebraic equations in 2(N = 4N) unknown displacement discontinuity components are obtained as:

$$\begin{aligned} b_s^i &= \sum_{j=1}^{N} C_{ss}(i, j) D_s^j + \sum_{j=1}^{N} C_{sn}(i, j) D_n^j \\ b_n^i &= \sum_{j=1}^{N} C_{ns}(i, j) D_s^j + \sum_{j=1}^{N} C_{nn}(i, j) D_n^j, \quad i = 1, N \end{aligned} \tag{24}$$

The quantities b_s^i and b_n^i, standing for the known boundary values of stress and displacement and $C_{ss}(i, j)$, etc., are the corresponding influence coefficient [11, 12].

2.2. Supplementary and image solutions for displacements and stresses

Based on the notation given in Figure 3, the combined displacements $\overset{I}{u}_i+\overset{S}{u}_i$ are:

$$\begin{aligned}\overset{I}{u}_x+\overset{S}{u}_x=&\frac{-1}{4\pi(1-\nu)}\sum_{j=1}^{4}\{[(1-2\nu)\sin\beta\overset{I}{F}_{j2}-2(1-\nu)\cos\beta\overset{I}{F}_{j3}+\{(3-4\nu)(y\sin2\beta-\bar{y}\sin\beta)+\\&2y\sin2\beta\}\overset{I}{F}_{j4}+\{(3-4\nu)(y\cos2\beta-\bar{y}\cos\beta)-y(1-2\cos2\beta)\}\overset{I}{F}_{j5}+2y(y\sin3\beta-\\&\bar{y}\sin2\beta)\overset{I}{F}_{j6}-2y(y\cos3\beta-\bar{y}\cos2\beta)\overset{I}{F}_{j7}]D_{\bar{x}}^{j}+[(1-2\nu)\cos\beta\overset{I}{F}_{j2}+\\&2(1-\nu)\sin\beta\overset{I}{F}_{j3}-\{(3-4\nu)(y\cos2\beta-\bar{y}\cos\beta)-y\}\overset{I}{F}_{j4}+\{(3-4\nu)(y\sin2\beta-\\&\bar{y}\sin\beta)\overset{I}{F}_{j5}-2y(y\cos3\beta-\bar{y}\cos2\beta)\overset{I}{F}_{j6}-2y(y\sin3\beta-\bar{y}\sin2\beta)\overset{I}{F}_{j7}]D_{\bar{y}}^{j}\}\end{aligned}\tag{25}$$

$$\begin{aligned}\overset{I}{u}_y+\overset{S}{u}_y=&\frac{-1}{4\pi(1-\nu)}\sum_{j=1}^{4}\{[(1-2\nu)\cos\beta\overset{I}{F}_{j2}-2(1-\nu)\sin\beta\overset{I}{F}_{j3}-\{(3-4\nu)(y\cos2\beta-\bar{y}\cos\beta)+\\&y(1-2\cos2\beta)\}\overset{I}{F}_{j4}+\{(3-4\nu)(y\sin2\beta-\bar{y}\sin\beta)-2y\sin2\beta)\}\overset{I}{F}_{j5}+\\&2y(y\cos3\beta-\bar{y}\cos2\beta)\overset{I}{F}_{j6}+2y(y\sin3\beta-\bar{y}\sin2\beta)\overset{I}{F}_{j4}]D_{\bar{x}}^{j}+\\&[(1-2\nu)\sin\beta\overset{I}{F}_{j2}-2(1-\nu)\cos\beta\overset{I}{F}_{j3}-(3-4\nu)(y\sin2\beta-\bar{y}\sin\beta)\overset{I}{F}_{j4}\\&-\{(3-4\nu)(y\cos2\beta-\bar{y}\cos\beta)+y\}\overset{I}{F}_{j5}+2y(y\sin3\beta-\bar{y}\sin2\beta)\overset{I}{F}_{j6}-\\&2y(y\cos3\beta-\bar{y}\cos2\beta)\overset{I}{F}_{j7}]D_{\bar{y}}^{j}\}\end{aligned}\tag{26}$$

The stresses $\overset{I}{\sigma}_{ij}+\overset{S}{\sigma}_{ij}$ associated with these displacements are:

$$\begin{aligned}\overset{I}{\sigma}_{xx}+\overset{S}{\sigma}_{xx}=&\frac{-2G}{4\pi(1-\nu)}\sum_{j=1}^{4}\{[\overset{I}{F}_{j4}-3(\cos2\beta\overset{I}{F}_{j4}-\sin2\beta)\overset{I}{F}_{j5}+\{2y(\cos\beta-3\cos3\beta)+\\&3\bar{y}\cos2\beta)\}\overset{I}{F}_{j6}+3\bar{y}\sin2\beta\}\overset{I}{F}_{j7}-2y(y\cos4\beta-\bar{y}\cos3\beta)\overset{I}{F}_{j8}-2y(y\sin4\beta-\\&\bar{y}\sin3\beta)\overset{I}{F}_{j9}]D_{\bar{x}}^{j}+[\overset{I}{F}_{j5}+\{2y(\sin\beta-2\sin3\beta)+3\bar{y}\sin2\beta)\}\overset{I}{F}_{j6}-\{2y(\cos\beta-2\cos3\beta)+\\&3\bar{y}\cos2\beta\}\overset{I}{F}_{j7}-2y(y\sin4\beta-\bar{y}\sin3\beta)\overset{I}{F}_{j8}+2y(y\cos4\beta-\bar{y}\cos3\beta)\overset{I}{F}_{j9}]D_{\bar{y}}^{j}\}\end{aligned}\tag{27}$$

$$\begin{aligned}\overset{I}{\sigma}_{yy}+\overset{S}{\sigma}_{yy}=&\frac{-2G}{4\pi(1-\nu)}\sum_{j=1}^{4}\{[\overset{I}{F}_{j4}-(\cos2\beta\overset{I}{F}_{j4}-\sin2\beta)\overset{I}{F}_{j5}-(4y\sin2\beta-\bar{y}\cos2\beta)\}\overset{I}{F}_{j6}+\\&(4y\sin\beta\cos2\beta+\bar{y}\sin2\beta\}\overset{I}{F}_{j7}+2y(y\sin4\beta-\bar{y}\sin3\beta)\overset{I}{F}_{j9}]D_{\bar{x}}^{j}+\\&[\overset{I}{F}_{j5}-\{2y\sin\beta-\bar{y}\sin2\beta)\overset{I}{F}_{j6}+(2y\cos\beta-\bar{y}\cos2\beta)\overset{I}{F}_{j7}+\\&2y(y\sin4\beta-\bar{y}\sin3\beta)\overset{I}{F}_{j8}-2y(y\cos4\beta-\bar{y}\cos3\beta)\overset{I}{F}_{j9}]D_{\bar{y}}^{j}\}\end{aligned}\tag{28}$$

$$\overset{I}{\sigma}_{xy}+\overset{S}{\sigma}_{xy}=\frac{-2G}{4\pi(1-\nu)}\sum_{j=1}^{4}\{[\sin 2\beta\overset{I}{F}_{j4}+(\cos 2\beta\overset{I}{F}_{j4}+\{2y\sin\beta(1+4\cos 2\beta)-\bar{y}\sin 2\beta\}\overset{I}{F}_{j6}+\{2y\cos\beta(3-4\cos 2\beta+\bar{y}\sin 2\beta\}\overset{I}{F}_{j7}+2y(y\sin 4\beta-\bar{y}\sin 3\beta)\overset{I}{F}_{j8}-2y(y\cos 4\beta-\bar{y}\cos 3\beta)\overset{I}{F}_{j9}]D_{\bar{x}}^{j}+[(4y\sin\beta\sin 2\beta+\bar{y}\cos 2\beta)\overset{I}{F}_{j6}-(4y\sin\beta\cos 2\beta-\bar{y}\sin 2\beta)\overset{I}{F}_{j7}-2y(y\cos 4\beta-\bar{y}\cos 3\beta)\overset{I}{F}_{j8}-2y(y\sin 4\beta-\bar{y}\sin 3\beta)\overset{I}{F}_{j9}]D_{\bar{y}}^{j}\} \quad (29)$$

where,

$$\overset{I}{\mathrm{F}}_{j8}=\overset{I}{\mathrm{F}}_{j8}(\bar{x}',\bar{y}')=\overset{I}{\mathrm{F}}_{j,\bar{x}'\bar{y}'\bar{y}'}=\frac{\partial^4\overset{I}{\mathrm{F}}_{j}(\bar{x}',\bar{y}')}{\partial\bar{x}'\partial\bar{y}'^3}\qquad \overset{I}{\mathrm{F}}_{j9}=\overset{I}{\mathrm{F}}_{j,\bar{y}'\bar{y}'\bar{y}'}=\frac{\partial^4\overset{I}{\mathrm{F}}_{j}(\bar{x}',\bar{y}')}{\partial\bar{y}'^4} \quad (30)$$

3. Verification of FD/BEM (proposed model)

The analytical solution to the Mindlin problem for shallow excavations [29] and the finite difference solution to the subsidence of a coal mine (Mazino coal mine) [30] were used for the verification of the proposed finite difference/boundary element method (FD/BEM).

3.1. Tangential stresses on surface of a shallow circular tunnel

In shallow excavations (the Mindlin problem), computation of tangential stresses on the surface is very important. To achieve this, a finite difference algorithm is added to the semi-infinite displacement discontinuity method using the cubic displacement discontinuity formulations (the proposed numerical method). It is assumed that the tunnel is of circular cross-section, and is driven at a shallow depth below a stress-free ground surface. The Mindlin problem shown in Figure 4 was numerically solved by the proposed method assuming a circular tunnel with D = 2R = diameter of the circular cavity = 2 m, C = depth of the cavity center (variable), E = Young modulus = 10 GPa, ν = Poisson's ratio = 0.2, σ_h = horizontal stress (far field stress) = –10 MPa, C/R = ratio of the depth of the cavity to its radius (R).

The analytical solution to this problem is due to Mindlin (1939). The displacement discontinuity program for the semi-infinite plane elasticity problems using cubic elements (SEMICDDM) was used for the solution of the same problem. Three different cases were considered, i.e. (i) C/R = 1.19, (ii) C/R =1.54, and (ii) C/R = 5.

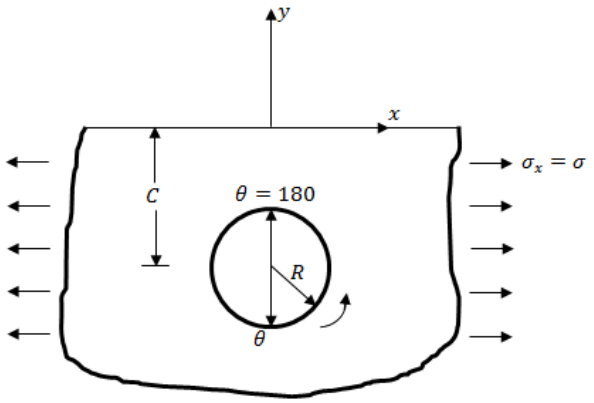

Figure 4. Mindlin problem for shallow tunnels [29].

Figure 5 shows the comparison between the approximate and exact values for the normalized tangential stress, σ_{xx}/σ_h, using different numbers of elements along the tunnel boundary (for C/R = 1.54). This Figure shows that as the number of elements along the boundary increases, the difference between the numerical and analytical values decreases.

Therefore, in the rest of the calculations, the number of elements may be fixed at 90. The analytical and numerical values for the normalized tangential stress, σ_{xx}/σ_h, for the three different cases are compared in Figures 6-8. These Figures show the variation in the tangential stress on the ground surface of the shallow tunnels due to the changes in depth (i.e. for different C/R ratios).

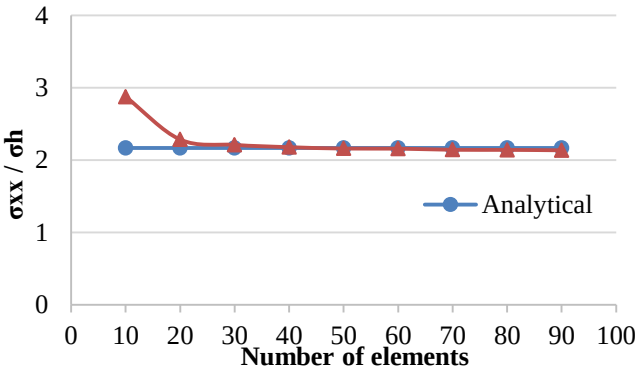

Figure 5. Comparison between approximate (numerical) and exact values for normalized tangential stress, σ_{xx}/σ_h, using different numbers of elements along tunnel boundary (for C/R = 1.54).

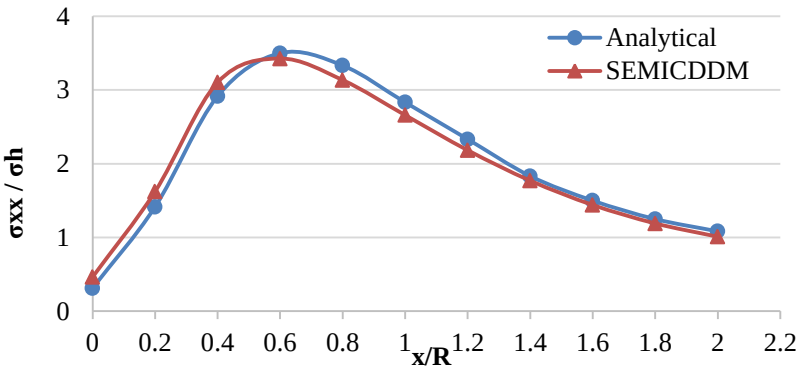

Figure 6. Comparison between approximate (numerical) and exact values for σ_{xx}/σ_h along x axis (i.e. on ground surface of shallow tunnel) for C/R = 1.19.

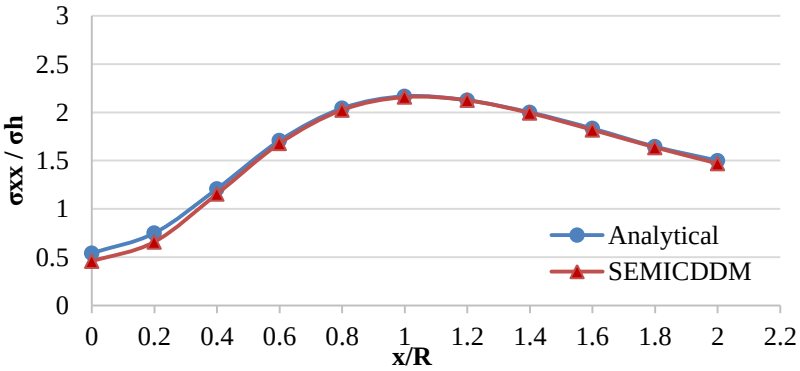

Figure 7. Comparison between approximate (numerical) and exact values for σ_{xx}/σ_h along x axis (i.e. on ground surface of shallow tunnel) for C/R = 1.54.

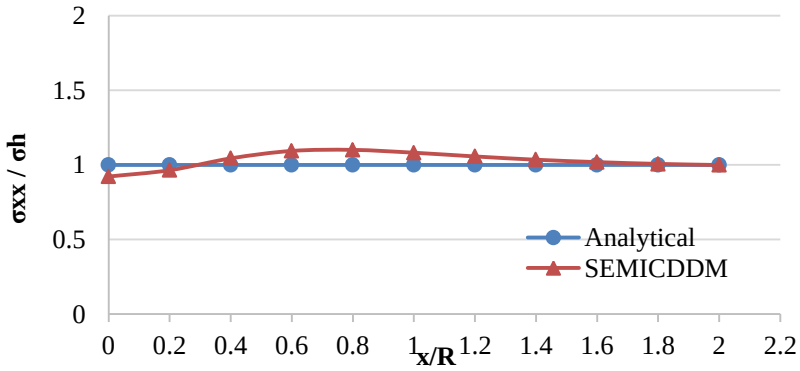

Figure 8. Comparison between approximate (numerical) and exact values for σ_{xx}/σ_h along x axis (i.e. on ground surface of shallow tunnel) for C/R =5.

3.2. Subsidence of Mazino longwall mine (Tabas)

The numerical modeling of a longwall mine subsidence [30] solved by a 3D finite difference method (FLAC^{3D} code) was compared with the numerical results obtained using the proposed FD/BEM (SEMICDDM code). Najafi et al. [30] have modeled the surface subsidence due to coal mine panels at a depth of 200 m in Mazino, Tabas, Iran. This surface subsidence was due to mining two adjacent longwall panels with a series of chain pillars (72.5 m in width) (Figure 9). The geometrical and geomechaincal characteristics of the Mazino longwall coal mine are presented in the Table 1 [30].

The maximum surface subsidence given by Najafi et al. was 42 cm. The same problem was modeled using the SEMICDDM code, and the maximum surface subsidence was estimated as 42.5 cm. The resulting surface subsidence diagrams were compared in Figure 10.

Therefore, the accuracy of the SEMICDDM code was validated by comparing its results with the corresponding results obtained analytically (the Mindlin problem) or numerically (FLAC^{3D} code).

Table 1. Characteristic of Mazino longwall mine [30].

Panel Width (m)	220	
Panel Length (m)	1200	
Layer Depth (m)	200	
Layer Thickness (m)	2.5	
Layer Inclination (Deg)	0 (Horizontal)	
Chain Pillar Width (m)	72.5	
	Embedded Rock	**Coal**
Young Modulus (GPa)	3.5	3
Density (ton/m^3)	2.6	1.6
Poisson's Ratio	0.3	0.29
Friction angle (Deg)	32	23
Cohesion (MPa)	4.7	0.5

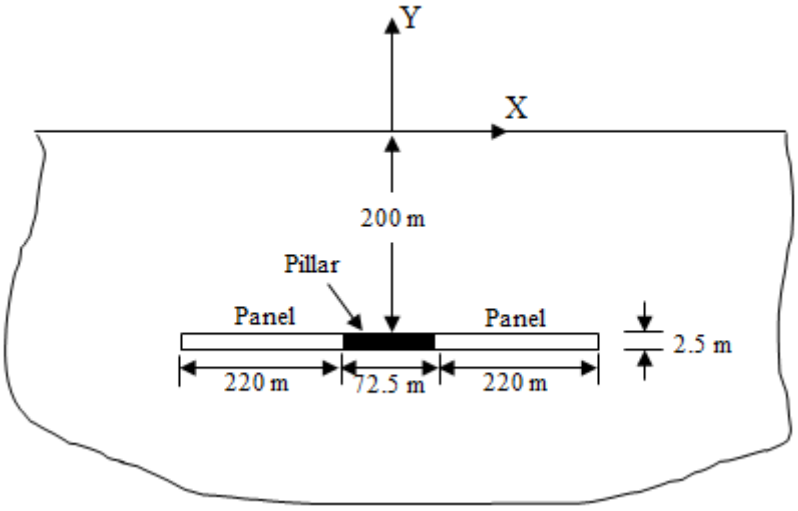

Figure 9. A schematic view of Mazino longwall coal mine [30].

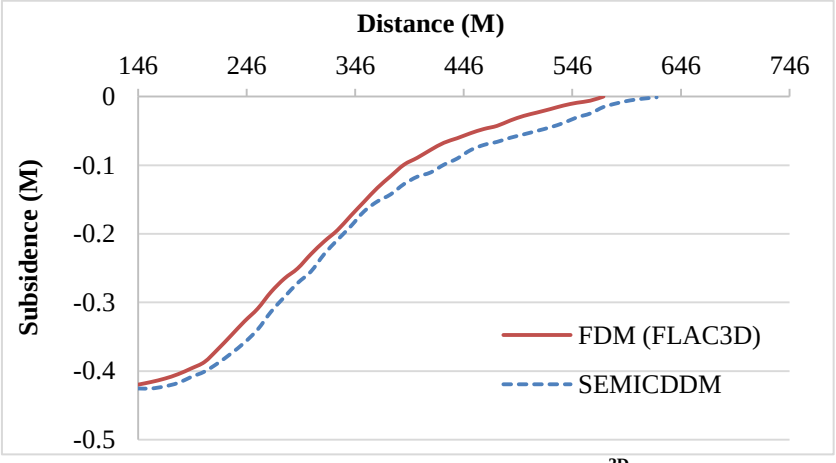

Figure 10. Comparing surface subsidence diagrams obtained by FLAC^{3D} and SEMICDDM codes in Mazino longwall mine.

4. Ground subsidence and horizontal strain of West Panel No. 3 of Parvadeh I in Tabas Coal Mine

As a practical application of the proposed modeling, the hybridized method was used for the subsidence analysis of an underground coal mining (Panel No. 3 of Parvadeh I in Tabas coal mine located in the central part of Iran) (Figure 11). Table 2 gives some of the characteristics of this mine [31].

The higher order displacement discontinuity method was hybridized with the classical finite difference method using the cubic displacement discontinuity variations along each boundary element to estimate the vertical displacements (subsidence) on the ground surface of Panel No. 3 (Figure 12).

Figure 12 shows the maximum surface subsidence due to extraction of the West Panel No. 3 of Parvadeh 1 Tabas Coal Mine (which is about 46 cm). The effect of the coal seam dip on the magnitude of the surface subsidence is also presented in this Figure. The magnitude of the surface subsidence on the left side of the diagram is slightly greater than the right side one, which is due to the inclination of the coal seam (14 degrees on the left side). It should be noted that if the coal seam was flat, then both sides of the subsidence diagram would be symmetric with respect to the y-axis.

The proposed numerical method was also used to predict the horizontal strain variations along the ground surface of the above-mentioned panel using the forward, central, and backward formulations given in Equations 15-17 (Figure 13).

Table 2. Characteristic of Parvade I in Tabas Coal mine (C1 Layer) [31].

Panel Width (m)	207	
Layer Depth (m)	357	
Layer Thickness (m)	2	
Layer Inclination (Deg)	14.24	
	Embedded Rock	**Coal**
Young Modulus (GPa)	2	1.5
Density (ton/m^3)	2.5	1.5
Poisson's Ratio	0.3	0.3

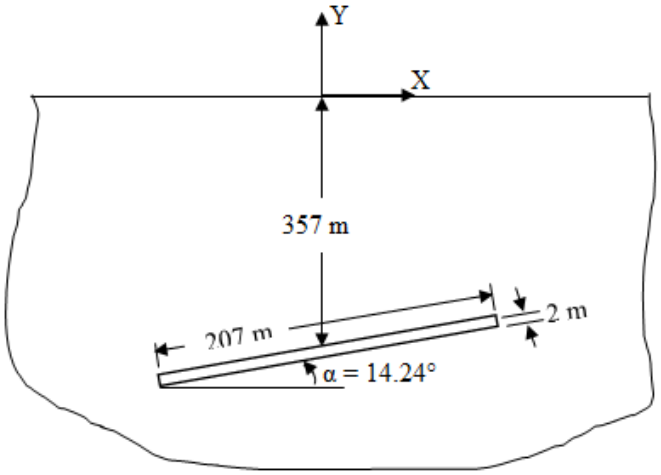

Figure 11. A schematic view of Panel No. 3 of Parvadeh I in Tabas coal mine.

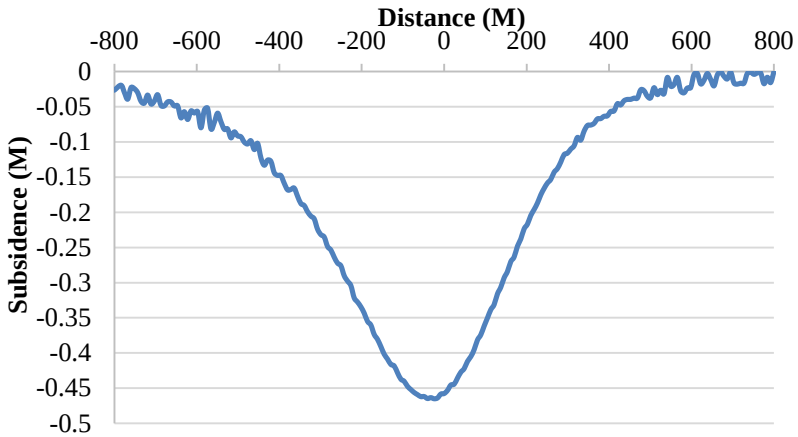

Figure 12. Ground subsidence diagrams using proposed method for West Panel No. 3 of Parvade I in Tabas Coal Mine (coal seam inclination is about 14 degrees).

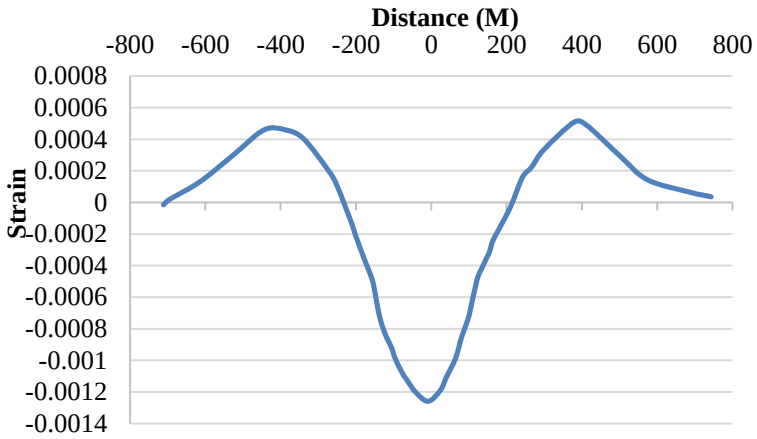

Figure 13. Horizontal strain diagrams using proposed method for West Panel No. 3 of Parvade I Tabas Coal Mine (coal seam inclination is about 14 degrees).

Figures 13 shows that the magnitude of the minimum horizontal strain on the surface due to extraction of the West Panel No. 3 of Parvadeh 1 Tabas Coal Mine is about –0.0012, taking place near the center of coal seam. At about 400 m on both sides of the center of coal seam, the maximum horizontal strain on the ground surface may take place. The magnitude of the maximum horizontal strain is about 0.0005, and it is almost the same at both sides of the coal seam. The negative values for the horizontal strain at the center of this diagram illustrate that the central part of the seam ground surface is under compression. At a distance about 400 m far from this center on both sides, the strain is positive, and, therefore, this part is under tension. Finally, at a distance about 700 m far from the center of this seam (on both sides), the horizontal strain tends to zero (which is trivial).

5. Analysis of geometrical and geomechanical effects on subsidence phenomenon

The main objective of this part is to study the ground subsidence behavior by changing the different parameters affecting this phenomenon. Therefore, the effects of the geometrical and geomechanical features of the model on the surface subsidence of a coal seam are analyzed numerically using the SEMICDDM code. Some of the input parameters taken from the results are presented in Table 2.

5.1. Effect of coal seam dip

The proposed numerical method was used for the analysis of the subsidence and horizontal strains for inclined seams at various dips. Considering the inclined seams at the dip angles of 30, 45, and 60 degrees with the same specifications given in Table 2, the effects of seam inclinations on the vertical displacements and horizontal strains on the ground surface of the excavation were estimated.

The effects of the coal seam dip angles on the subsidence and horizontal strains are shown graphically in Figures 14 and 15 for the dip angles of 14 (current dip), 30, 45, and 60 degrees, respectively.

Figure 14 illustrates that with increase in the seam inclination, the maximum surface subsidence decreases. On the other hand, by increasing the seam inclination, especially greater than 45 degrees, the subsidence basin tilts toward the left side of the dip direction.

Figure 15 illustrates that with increase in the seam dips (from 14 to 45 degrees), the tensional part of the strain diagram does not change sharply, while the horizontal strain decreases meaningfully in the compressive part of this diagram. By increasing the seam dip from 45 to 60 degrees, the magnitude of the strain in the tensional part of the diagram decreases. This may be because as the dip angle increases from 45 to 60 degrees, the seam becomes almost vertical.

5.2. Effect of Young modulus

Considering the characteristics given in Table 2, the effects of variation in the rock properties such as Young modulus (E) on the subsidence phenomenon are illustrated in Figures 16-18 (assuming a subsided rock mass with many different Young moduli). The effect of Young modulus (E) on subsidence (vertical surface displacement) is given in Figures 16 and 17. Figure 16 shows the subsidence diagrams for the Young modulus changing from E = 2 GPa (current Young modulus) to E = 0.5 GPa, while Figure 17 shows the same diagrams for the Young modulus changing from E = 2 GPa (current Young modulus) to E = 4 GPa.

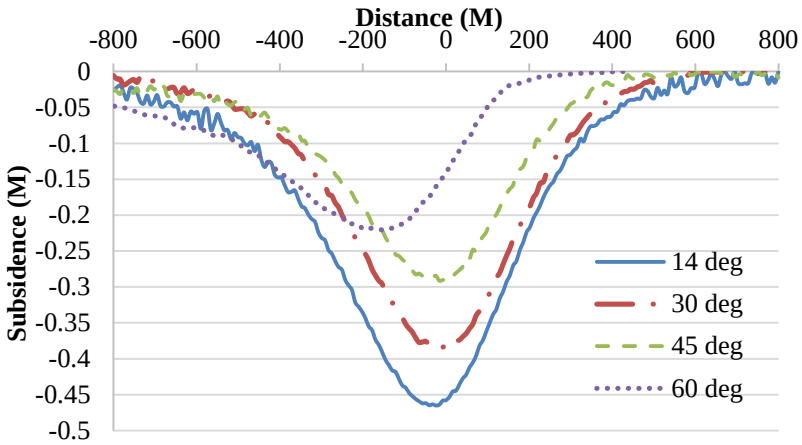

Figure 14. Subsidence diagrams numerically estimated for a coal seam with dip angles of α = 14, 30, 45, and 60 degrees.

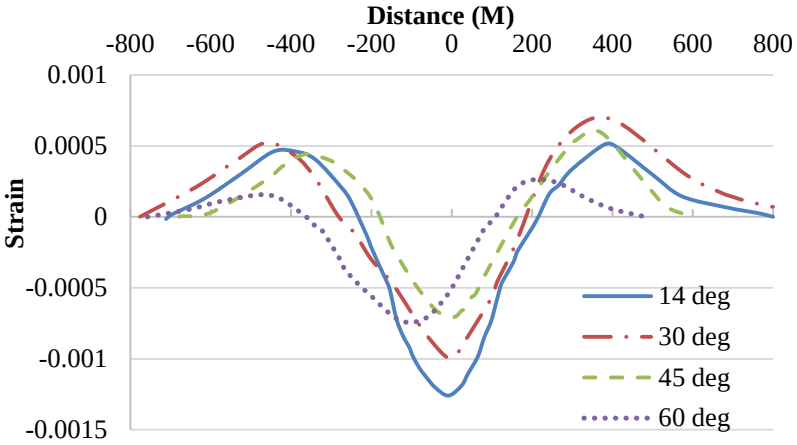

Figure 15. Horizontal strain diagrams numerically estimated for a coal seam with dip angles of α = 14, 30, 45, and 60 degrees.

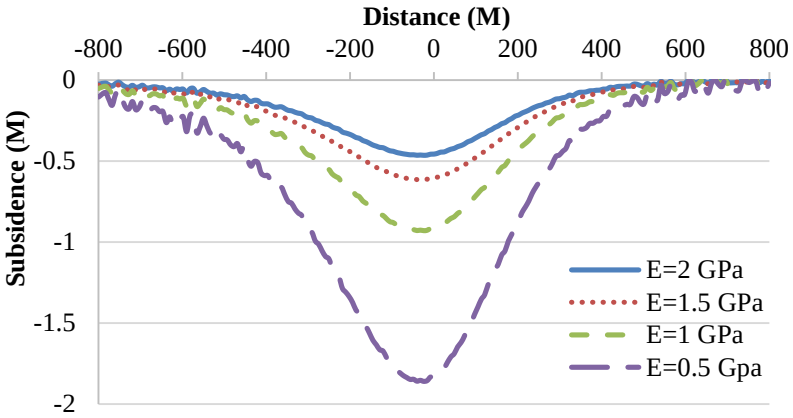

Figure 16. Subsidence diagrams numerically estimated for a rock with different Young modulus (E = 0.5-2 GPa).

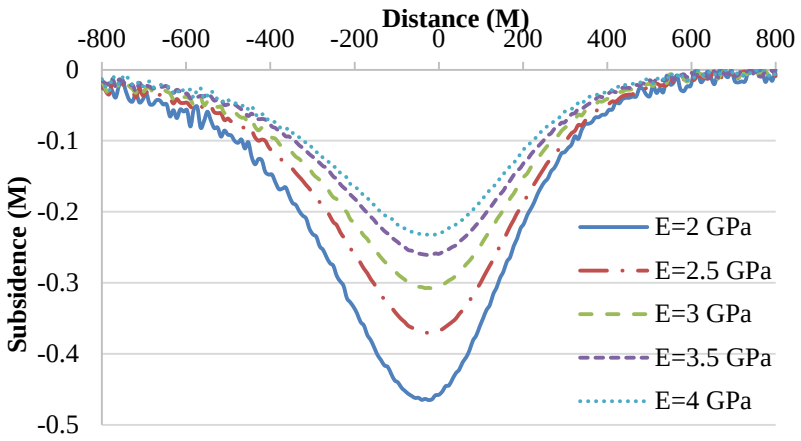

Figure 17. Subsidence diagrams numerically estimated for a rock with different Young moduli (E = 2-4 GPa).

Figures 16 and 17 illustrate that an increase in the value of Young modulus leads to a decrease in the subsidence. Especially at low values of Young modulus (E = 0.5 to E = 1 GPa), the subsidence decreases sharply (which means that the effect of Young modulus on weak rock masses is more important). The effects of Young modulus (E) on the horizontal surface strains are given in Figure 18.

Figure 18 shows that a decrease in the Young modulus leads to an increase in the magnitude of the horizontal strain in both parts of this diagram.
Comparing Figures 14 to 18 illustrate that the variation in Young modulus only has a particular influence on the magnitude of the subsidence and horizontal strain, while variation in seam dip in addition to the changes in the magnitude of subsidence and horizontal strain will also change the location of both the maximum subsidence and the maximum and minimum horizontal strains.

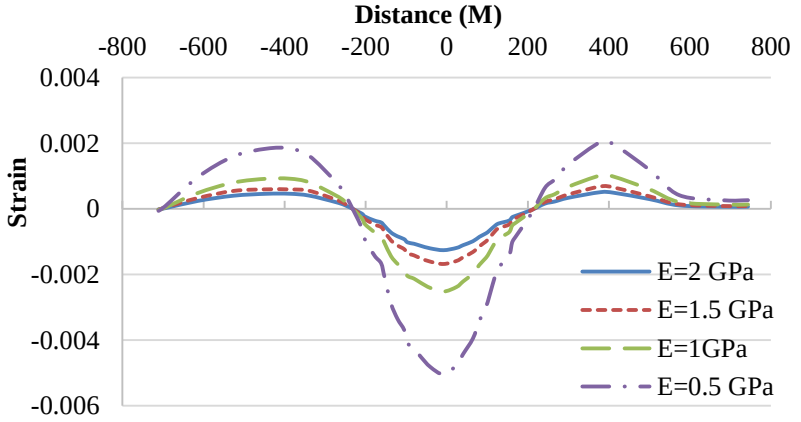

Figure 18. Horizontal surface strain diagrams numerically estimated for a rock with different Young moduli (E = 0.5-2 GPa).

5.3. Effect of excavation depth

Effects of depth of coal seam on the vertical displacement and horizontal strain curves of the example problem stated in Table 2 may be estimated as shown in Figures 19 and 20 for 357, 257, and 157 m seam depths, respectively.
As deduced from Figure 19, the effect of seam depth on the vertical surface displacement is clear. As the coal layer gets closer to the surface, the magnitude of the maximum surface subsidence is greater. Especially when the seam is very close to the surface, this effect is more visible.
Figure 20 shows that the horizontal surface strain sharply decreases as the depth of excavation increases. Therefore, as the seam gets closer to the surface, the magnitude of the horizontal strain is greater.

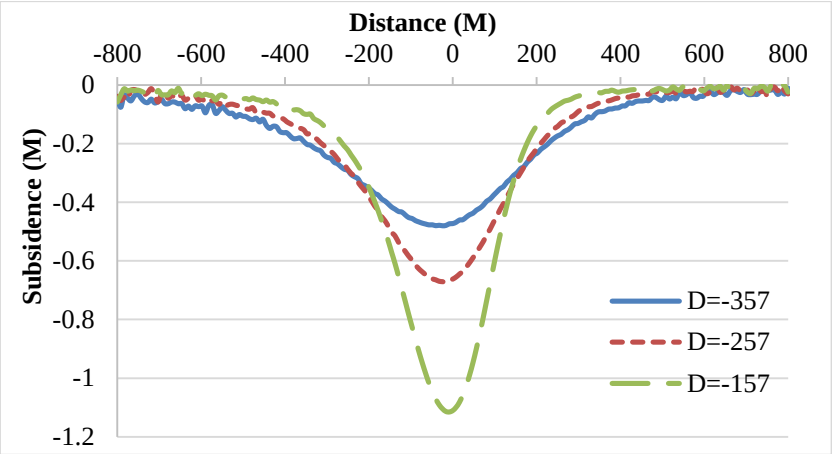

Figure 19. Subsidence diagrams numerically estimated for an excavated coal seam at depths of 357, 257, and 157 m below subsided ground surface.

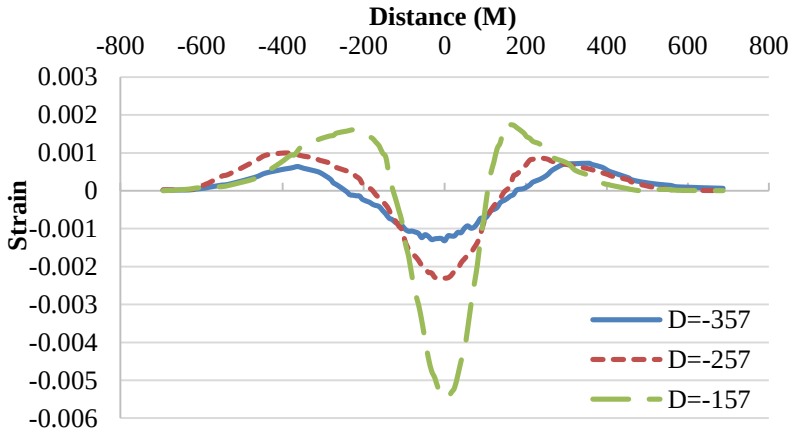

Figure 20. Horizontal strain diagrams numerically estimated for an excavated coal seam at depths of 357, 257, and 157 m below subsided ground surface.

5. Conclusions

A higher order indirect boundary element method hybridized using the classical finite difference method to predict the subsidence and horizontal strains (or stresses) is involved in underground excavations. The basic formulations and numerical procedure were explained briefly. Some example problems were numerically solved by the proposed hybridized FD/BEM. The first example was that of a circular shallow tunnel (Mindlin problem), and the second one was from the field (Mazino coal mine). The numerical results obtained by solving these examples were compared with the corresponding analytical and numerical results cited in the literature. These comparisons showed that the proposed numerical method could predict the subsidence and horizontal strain component on the ground surface by a good approximation. The effects of coal seam inclination angles and depths, and rock properties on the subsidence and horizontal strains of the West Panel No. 3 of Parvade I in Tabas Coal Mine (C1 Layer) were numerically analyzed by the proposed numerical method. It was shown that the coal seam dip angles, the seam depth, and the elastic modulus of the rock all changed the magnitude and trend of both the subsidence and horizontal strains. It should be noted that the boundary of the subsided area tends to infinity or is limited for the case of using the numerical method, and therefore, the truncation error may be omitted.

References

[1]. National Coal Board. (1966, revised 1975). Subsidence Engineers' Handbook. The Board. London.

[2]. Whittaker, B.N. and Reddish, D.J. (1984). Mining subsidence in long wall mining with special reference to the
prediction of surface strains. Proceeding 2nd International Conference on Stability in Underground Mining. Lexington. Kentucky. 6-8 August. pp. 576-588.

[3]. Whittaker, B.N., Reddish, D.J. and Fitzpatrick, D.J. (1985). Calculation by computer program of mining

subsidence grounds strain patterns due to multiple long wall extractions. Min Sci & Techn. 3: 21-33.

[4]. Whittaker, B.N. and Reddish, D.J. (1989). Subsidence, Occurrence, Prediction and Control. Elsevier. Amsterdam. Netherlands.

[5]. Alejano, L., Ramírez-Oyanguren, L. and Taboada, J. (1999). FDM predictive methodology for subsidence due to flat and inclined coal seam mining. Int J Rock Mech Min Sci. 36 (4): 475-491.

[6]. Elashiry, A.A., Gomma, W.A. and Imbaby, S.S. (2009). Numerical modelling of surface subsidence induced by underground phosphate mines at abu-tatur area. J Eng Sci. 37 (3): 699-709.

[7]. Islam, M.R., Hayashi, D. and Kamruzzaman, A.B.M. (2009). Finite element modeling of stress distributions and problems for multi-slice longwall mining in Bangladesh, with special reference to the Barapukuria coal mine. Int. J. Coal Geol. 78 (2): 91-109.

[8]. Nuric, A., Nuric, S., Kricak, L., Lapandic, I. and Husagic, R. (2012). Numerical Modeling and Computer Simulation of Ground Movement Above Underground Mine. World Academy of Science. Engineering and Technology. 6 (9): 361-369.

[9]. Xu, N., Kulatilake, P.H.S.W., Tian, H., Wu, X., Nan, Y. and Wei, T. (2013). Surface subsidence prediction for the WUTONG mine using a 3-D finite difference method. Comput Geotech. 48: 134-145.

[10]. Helm, P.R., Davie, C.T. and Glendinning, S. (2013). Numerical modelling of shallow abandoned mine working subsidence affecting transport infrastructure. Eng Geo. 154: 6-19.

[11]. Crouch, S.L. and Starfield, A. M. (1983). Boundary Element Methods in Solid Mechanics. Allen and Unwin. London.

[12]. Scavia, C. (1995). A Method for the Study of Crack Propagation in Rock Structures. Geotehcnique. 45 (3): 447-463.

[13]. Aliabadi, M.H. (1998). Fracture of rocks. Computational Mechanics Publications. Southampton. U.K.

[14]. Stephansson. O. (2002). Recent Rock Fracture Mechanics Developments. 1st Iranian Rock Mechanics Conference. Tehran. Iran. 29-30 January. pp. 675-698.

[15]. Katsikadelis, J.T. (2002). Boundary elements theory and applications. Elsevier.

[16]. Fatehi Marji, M., Hosseini Nasab, H. and Kohsary, A.H. (2006). On the uses of special crack tip elements in numerical fracture mechanics. Int J Solids Struct. 43: 1669-1692.

[17]. Fatehi Marji, M. (2014). Numerical analysis of quasi-static crack branching in brittle solids by a modified displacement discontinuity method. Int. J. Solids Struct. 51 (9): 1716-1736.

[18]. Fatehi Marji, M. and Dehghani, I. (2010). Kinked crack analysis by a hybridized boundary element/boundary collocation method. Int J Solids Struct. 47: 922-933.

[19]. Fatehi Marji, M. and Dabbagh, A. (2011). On the horizontal strain analysis of the subsidence phenomenon by a hybridized boundary element/finite difference method. International Multidisciplinary Scientific Geo-conference & Expo (SGEM 2011). Albena. Bulgaria. 19-25 June.

[20]. Fatehi Marji, M. (2013). On the use of power series solution method in the crack analysis of brittle materials by indirect boundary element method. Eng Frac Mech. 98: 365-382.

[21]. Shen, B., Stephansson, O. and Rinne, M. (2014). Modelling Rock Fracturing Processes A Fracture Mechanics Approach Using FRACOD. Springer.

[22]. Abdollahipour, A., Fatehi Marji, M., YarahmadiBafghi, A. and Gholamnejad, J. (2015). Simulating the propagation of hydraulic fractures from a circular wellbore using the Displacement Discontinuity Method. Int J Rock Mech Min Sci. 80: 281-291.

[23]. Abdollahipour, A., Fatehi Marji, M., Yarahmadi Bafghi, A.R. and Gholamnejad, J. (2016). Numerical investigation of effect of crack geometrical parameters on hydraulic fracturing process of hydrocarbon reservoirs. Journal of Mining and Environment. 7 (2): 205-214.

[24]. Chen, J.T. and Hong, H.K. (1999). Review of dual boundary elements methods with emphasis on hyper singular integrals and divergent series. App Mech Rev. 52 (1): 17-33.

[25]. Hosseini Nasab, H. and Fatehi Marji, M. (2007). A Semi-infinite Higher Order Displacement Discontinuity Method and Its Application to the Quasi-static Analysis of Radial Cracks Produced by Blasting. J Mech Mater Stru. 2 (3): 439-458.

[26]. Fatehi Marji, M., Goshtasbi, K., Gholamnejad, J. and Haeri, H. (2010). On the displacement discontinuity analysis of radial cracks emanating from circular blast holes in rock blasting. ISRM International and 6th Asian Rock Mechanics Symposium. New Delhi. India. 23-27 October.

[27]. Fatehi Marji, M. and Eghbal M. (2011). Simulating the failure mechanism of rock slopes (due to kinked and secondary cracks propagation) by a higher order displacement discontinuity method. 12th ISRM Rock Mechanics Symposium. Beijing. China. 16-21 October.

[28]. Fatehi Marji, M. and Manouchehrian, M.A. (2012). Comparison of indirect boundary element and finite element methods. A case study: Shiraz-Esfahan railway tunnel in Iran. Fron Struc Civ Eng. 6: 365-368.

[29]. Mindlin, R.D. (1939). Stress distribution around a tunnel. Proceedings of the American Society of Civil Engineers. 65 (4): 619-642.

[30]. Najafi, M. and Ataee, M. (2012). Surface subsidence prediction due to mechanized longwall mining by a numerical modeling, case study: Tabas coal mine. 1st iranian coal Congress. Shahrood. Iran. 29-31 August. (Persian).

[31]. ADAM Co. (1992). Tabas Coal Mining Project. Mine No 1.

Appendix

The integral and derivatives of the common cubic integral, $I_4(x,y)$

$$I_4(x,y)=\int_{-a}^{a}\varepsilon^3\ln\left[(x-\varepsilon)^2+y^2\right]^{\frac{1}{2}}d\varepsilon=-xy(x^2-y^2)(\theta_1-\theta_2)+0.25(3x^4-6x^2y^2+$$

$$8a^2x^2+a^4-y^4)\left[\ln(r_1)-\ln(r_2)\right]-2ax(x^2+a^2)\left[\ln(r_1)+\ln(r_2)\right]+1.5ax^3-3axy^2+7a^3x/6$$

Let $C_1=-xy(x^2-y^2)$, $C_2=0.25(3x^4-6x^2y^2+8a^2x^2+a^4-y^4)$, $C_3=-2ax(x^2+a^2)$, $C_4=1.5ax^3-3axy^2+7a^3x/6$ and $L=\left[\ln(r_1)+\ln(r_2)\right]$.

Therefore,

$C_{1,x}=-3x^2y+y^3$, $C_{1,y}=-x^3+3xy^2$, $C_{1,xy}=-3x^2+3y^2$, $C_{1,yy}=6xy$, $C_{1,xyy}=6y$, $C_{1,yyy}=6x$

$C_{2,x}=3x^3-3xy^2+4a^2x$, $C_{2,y}=-(3x^2y+y^3)$, $C_{2,xy}=-6xy$, $C_{2,yy}=-3(x^2+y^2)$, $C_{2,xyy}=-6x$, $C_{2,yyy}=-6y$;

$C_{3,x}=-6ax^2-2a^3$, $C_{3,y}=0$, $C_{4,x}=4.5ax^3-3ay^2+7a^3/6$, $C_{4,y}=-6axy$, $C_{4,xy}=6ay$, $C_{4,yy}=-6ax$, $C_{4,xyy}=-6a$, $C_{4,yyy}=0$

$$L_{,x}=-\left(\frac{(x-a)}{r_1^2}+\frac{(x+a)}{r_2^2}\right),\ L_{,y}=-\left(\frac{y}{r_1^2}+\frac{y}{r_2^2}\right),\ L_{,xy}=2y\left(\frac{(x-a)}{r_1^4}+\frac{(x+a)}{r_2^4}\right),\ L_{,yy}=-\left(\frac{(x-a)^2-y^2}{r_1^4}+\frac{(x+a)^2-y^2}{r_2^4}\right),$$

$$L_{,yyy}=-2\left(\frac{(x-a)(r_1^2-4y^2)}{r_1^6}+\frac{(x+a)(r_2^2-4y^2)}{r_2^6}\right),\ L_{,xyy}=-2y\left(\frac{3(x-a)^2-y^2}{r_1^6}+\frac{3(x+a)^2-y^2}{r_2^6}\right),$$

$$I_4(x,y)=C_1I_{0,y}+C_2I_{0,x}+C_3L+C_4$$

$$I_{4,x}=C_{1,x}I_{0,y}+C_1I_{0,xy}+C_{2,x}I_{0,x}+C_2I_{0,xx}+C_{3,x}L+C_3L_{,x}+C_{4,x}$$

$$I_{4,y}=C_{1,y}I_{0,y}+C_1I_{0,yy}+C_{2,y}I_{0,x}+C_2I_{0,xy}+C_3L_{,y}+C_{4,y}$$

$$I_{4,xy}=C_{1,xy}I_{0,y}+C_{2,xy}I_{0,x}+(C_{1,y}+C_{2,x})I_{0,xy}+(C_{1,x}-C_{2,y})I_{0,yy}+C_1I_{0,xyy}-C_2I_{0,yyy}+C_{3,x}L_{,y}+C_3L_{,xy}+C_{4,xy}$$

$$I_{4,yy}=C_{1,yy}I_{0,y}+C_{2,yy}I_{0,x}+2C_{1,y}I_{0,yy}+2C_{2,y}I_{0,xy}+C_1I_{0,yyy}+C_3L_{,yy}-6ax$$

$$I_{4,xyy}=C_{1,xyy}I_{0,y}+C_{2,xyy}I_{0,x}+(C_{1,yy}+2C_{2,xy})I_{0,xy}+(2C_{1,xy}-C_{2,yy})I_{0,yy}+$$

$$(2C_{1,y}+C_{2,x})I_{0,xyy}+(C_{1,x}-2C_{2,y})C_2I_{0,yyy}+C_1I_{0,xyyy}-C_2I_{0,yyyy}+C_{3,x}L_{,yy}+C_3L_{,xyy}+C_{4,xyy}$$

$$I_{4,yyy}=6xI_{0,y}-6yI_{0,x}+18xyI_{0,yy}-9(x^2+y^2)I_{0,xy}+2C_{2,y}I_{0,xyy}+3C_{1,y}I_{0,yyy}+C_1I_{0,yyyy}+C_3L_{,yyy}$$

and for the semi-infinite plane case, the following derivatives are also needed:

$$I_{4,xyyy}=6I_{0,y}-12xI_{0,xy}+24yI_{0,yy}+18y^2I_{0,yyy}+(3C_{1,y}+C_{2,x})I_{0,xyyy}+$$

$$(C_{1,x}-3C_{2,y})I_{0,yyyy}+C_1I_{0,xyyyy}-C_2I_{0,yyyyy}+C_{3,x}L_{,yyy}+C_3L_{,xyyy}$$

$$I_{4,yyyy}=-6I_{0,x}-24yI_{0,xy}+24xI_{0,yy}-15(x^2+y^2)I_{0,xyy}+36xyI_{0,yyy}+2C_{2,y}I_{0,xyyy}$$

$$+4C_{1,y}I_{0,yyyy}+C_1I_{0,yyyyy}+C_3L_{,yyyy}$$

where,

$$I_{0,xyyyy}=24y\left(\frac{(x-a)((x-a)^2-y^2)}{r_1^8}-\frac{(x+a)((x+a)^2-y^2)}{r_2^8}\right)$$

$$I_{0,yyyyy}=\frac{I_{0,yyyy}}{y}-8y^2\left(\frac{5(x-a)^2-y^2}{r_1^8}-\frac{5(x+a)^2-y^2}{r_2^8}\right)$$

$$L_{,xyyy}=-\frac{I_{0,yyyy}}{y}+8y^2\left(\frac{5(x-a)^2-y^2}{r_1^8}+\frac{5(x+a)^2-y^2}{r_2^8}\right)$$

$$L_{,yyyy}=-24y\left(\frac{(x-a)\left[(x-a)^2-y^2\right]}{r_1^8}+\frac{(x+a)\left[(x+a)^2-y^2\right]}{r_2^8}\right)$$

تحلیل پدیده نشست سطح زمین ناشی از حفر فضاهای زیرزمینی با استفاده از روش ترکیبی المان مرزی/تفاضل محدود

سید اسماعیل میرسالاری، محمد فاتحی مرجی*، جواد غلام نژاد و مهدی نجفی

دانشکده مهندسی معدن و متالورژی، دانشگاه یزد، ایران

ارسال ۲۰۱۶/۵/۲۶، پذیرش ۲۰۱۶/۱۰/۳۰

* نویسنده مسئول مکاتبات: mohammad.fatehi@gmail.com

چکیده:

تحلیل تنش‌ها، جابجایی‌ها و کرنش‌های افقی ایجاد شده در پدیده نشست سطح زمین ناشی از حفریات زیرزمینی در سنگ‌ها می‌تواند توسط فرمولاسیون ترکیبی المان مرزی غیرمستقیم مرتبه بالا/تفاضل محدود (BE/FD) انجام شود. در این روش یک ناحیه نیمه بی‌نهایت با استفاده از المان‌های ناپیوستگی جابجایی درجه سوم مجزا سازی (عددی سازی) می‌شود (یعنی هر کدام از المان‌های مرتبه بالا به چهار زیر المان تقسیم می‌شوند که ناپیوستگی جابجایی درجه سه را نشان می‌دهند). سپس فرمولاسیون تفاضل محدود معمول (یعنی فرمولاسیون تفاضل محدود پسرو، میانی و پیشرو) با فرمولاسیون المان مرزی ترکیب می‌شود و ما را قادر به محاسبه تنش‌های مماسی و کرنش‌های افقی برای هر المان می‌سازد. چندین مسئله و مدل با این روش عددی حل شد و نتایج به دست آمده از آن با نتایج مرتبط موجود در مطالعات دیگران مقایسه شد. این مقایسه‌ها، مفید بودن و اعتبار روش پیشنهادی را نشان داد. به منظور بررسی مقبولیت روش ترکیبی پیشنهادی، یک مسئله کاربردی در زمینه نشست زمین نیز مدل‌سازی و اجرا شد.

کلمات کلیدی: نشست زمین، کرنش افقی، مسائل نیمه بی‌نهایت، روش المان مرزی غیرمستقیم، روش تفاضل محدود، المان‌های مرتبه بالا.